JACS
JOURNAL OF THE AMERICAN CHEMICAL SOCIETY
Article
pubs.acs.org/JACS

Ligand Aspect Ratio as a Decisive Factor for the Self-Assembly of Coordination Cages

Suzanne M. Jansze,[†,¶] Giacomo Cecot,[†,¶] Matthew D. Wise,[†] Konstantin O. Zhurov,[†] Tanya K. Ronson,[§] Ana M. Castilla,[§] Alba Finelli,[†] Philip Pattison,[#,⊥] Euro Solari,[†] Rosario Scopelliti,[†] Genrikh E. Zelinskii,[‡] Anna V. Vologzhanina,[‡] Yan Z. Voloshin,[‡] Jonathan R. Nitschke,*[,§] and Kay Severin*[,†]

[†]Institut des Sciences et Ingénierie Chimiques, École Polytechnique Fédérale de Lausanne (EPFL), CH-1015 Lausanne, Switzerland
[§]Department of Chemistry, University of Cambridge, Cambridge CB2 1EW, United Kingdom
[‡]Nesmeyanov Institute of Organoelement Compounds of the Russian Academy of Sciences, 119991 Moscow, Russia
[#]Laboratory of Crystallography, Ecole Polytechnique Fédérale de Lausanne (EPFL), CH-1015 Lausanne, Switzerland
[⊥]Swiss-Norwegian Beamline, ESRF, 38000 Grenoble, France

Supporting Information

ABSTRACT: It is possible to control the geometry and the composition of metallasupramolecular assemblies via the aspect ratio of their ligands. This point is demonstrated for a series of iron- and palladium-based coordination cages. Functionalized clathrochelate complexes with variable aspect ratios were used as rod-like metalloligands. A cubic $Fe^{II}_8L_{12}$ cage was obtained from a metalloligand with an intermediate aspect ratio. By increasing the length or by decreasing the width of the ligand, the self-assembly process resulted in the clean formation of tetrahedral $Fe^{II}_4L_6$ cages instead of cubic cages. In a related fashion, it was possible to control the geometry of Pd^{II}-based coordination cages. A metalloligand with a large aspect ratio gave an entropically favored tetrahedral $Pd^{II}_4L_8$ assembly, whereas an octahedral $Pd^{II}_6L_{12}$ cage was formed with a ligand of the same length but with an increased width. The aspect ratio can also be used to control the composition of dynamic mixtures of Pd^{II} cages. Out of two metalloligands with only marginally different aspect ratios, one gave rise to a self-sorted collection of $Pd^{II}_4L_8$ and $Pd^{II}_6L_{12}$ cages, whereas the other did not.

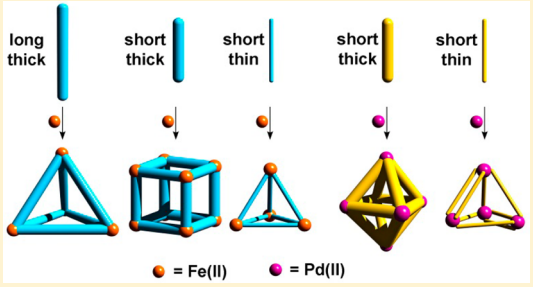

INTRODUCTION

The structural outcomes of metallasupramolecular self-assembly processes are largely controlled by the nature of the building blocks, i.e., metal ions, ligands, and possibly templates.[1] From a design perspective, the ligand is arguably the most important building block, because chemists can use the repertoire of synthetic chemistry to make a vast collection of ligands with diverse structures and properties.

By choosing an appropriate ligand, it is possible to influence the size, the geometry, and the functionality of the resulting metallasupramolecular assembly. Several factors are known to be of importance in this context. Structural rigidity of the ligand is a prerequisite for the assembly of polynuclear assemblies, because flexible ligands tend to favor complexes of low nuclearity. For rigid ligands, the distance and the relative orientation of the donor atoms are key parameters, allowing control of the size and geometry of the final assembly. This point is nicely illustrated by work from the Fujita group, who have explored the assembly of spherical coordination cages from bent dipyridyl ligands and Pd^{II} ions.[2] By slight variation of the bend angle, they were able to make $Pd^{II}_{12}L_{24}$ or $Pd^{II}_{24}L_{48}$ cages in a controlled fashion. The nature of the donor atom (e.g., oxygen vs nitrogen) and the charge of the ligand are likewise important parameters. For example, it is possible to make heteroleptic assemblies by mixing cis-blocked L_2MX_2 complexes (M = Pd or Pt; X = weakly coordinating anion) with neutral N-donor ligands and anionic carboxylate ligands.[1a,3] Taken together, the homoleptic $[L_2M(\text{N-donor})_2]^{2+}$ and $L_2M(O_2CR)_2$ complexes are thermodynamically less stable than the mixed $[L_2M(\text{N-donor})(O_2CR)]^{+}$ complex, resulting in the clean formation of heteroleptic assemblies.

Strategic functionalization of ligands with bulky groups can also be used to control the self-assembly behavior. For example, it is possible to favor heteroleptic complexes over homoleptic complexes by using two ligands, one of which has bulky groups in the vicinity of the donor atom(s).[4] In this case, the coordination of two bulky ligands to the same metal center is thermodynamically disfavored, pushing the system toward the formation of heteroleptic complexes. Steric interactions that are remote from the metal binding site have also been employed as an element of control,[5] but this strategy is less explored.

The investigation described herein deals with an underappreciated parameter in ligand design: the aspect ratio of a rigid rod-type ligand. We show that the length-to-width ratio of a ligand can be used to control the geometries of coordination

Received: December 17, 2015
Published: February 8, 2016

DOI: 10.1021/jacs.5b13190
J. Am. Chem. Soc. 2016, 138, 2046−2054

cages. In particular, we demonstrate that entropically disfavored cubic and octahedral cages are formed instead of tetrahedra if the aspect ratio of the ligand is reduced (Scheme 1).

Scheme 1. Rigid Rod-Type Ligands with Different Aspect Ratios Give Rise to Different Coordination Cages

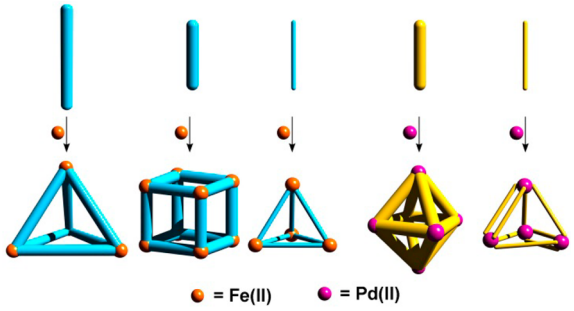

Furthermore, we have investigated the self-sorting behavior of ligands with variable aspect ratios. Minor differences in the length-to-width ratio were found to have a pronounced effect on the compositions of dynamic mixtures of cages.

RESULTS AND DISCUSSION

Clathrochelate Complexes as Metalloligands with a Variable Aspect Ratio. Clathrochelate complexes capped with boronate ester groups are formed by a metal-templated condensation reaction of a dioxime ligand with a boronic acid.[6] When Fe^{II} is employed as the metal template, the resulting complexes are diamagnetic, robust, and inert. Such clathrochelate complexes can easily be converted into metalloligands.[7] Different functional groups can be introduced by choosing an appropriate boronic acid (in particular, arylboronic acids),[8] and the lateral size and the solubility can be modulated by variation of the dioxime building block (Scheme 2). We note that numerous boronic acids and some dioximes are commercially available, and that the yields of clathrochelate syntheses are typically good.

Scheme 2. Clathrochelate Complexes as Robust, Flexible, and Easy-to-Access Metalloligands

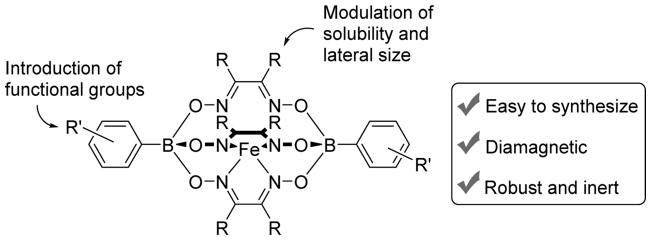

We and others have recently shown that clathrochelate complexes with apical pyridyl groups can be used as N-donor ligands in metallasupramolecular chemistry. Different molecular architectures have been synthesized, including macrocycles,[9] cages,[10] and metal−organic frameworks.[9b] Furthermore, pyridyl-capped clathrochelates have been used to bridge heterometallic Cr_7Ni rings. These complexes display interesting magnetic behavior.[11]

Clathrochelate-based metalloligands appear to be ideally suited to investigate the influence of the aspect ratio on self-assembly behavior. The length of the ligands can be modulated via the boronate ester cap, and the lateral size of the ligand can be varied by choosing an appropriate dioxime ligand. The iron center in clathrochelate complexes shows a distorted trigonal prismatic coordination geometry. Therefore, clathrochelates display approximate C_3 symmetry when viewed along the B···B axis. Functionalized clathrochelate complexes are thus intrinsically 3-dimensional metalloligands with rigid rod geometry.

For our investigation, we have focused on three types of coordination cages which are known to form with rigid rod ligands. $Fe^{II}_{2n}L_{3n}$ cages can be obtained from ligands with two terminal formylpyridine groups upon reaction with aminobenzene derivatives and an Fe^{II} salt (Scheme 3a).[12,13] In similar

Scheme 3. Fe^{II}- and Pd^{II}-Based Coordination Cages with Rigid Rod-Type Ligands

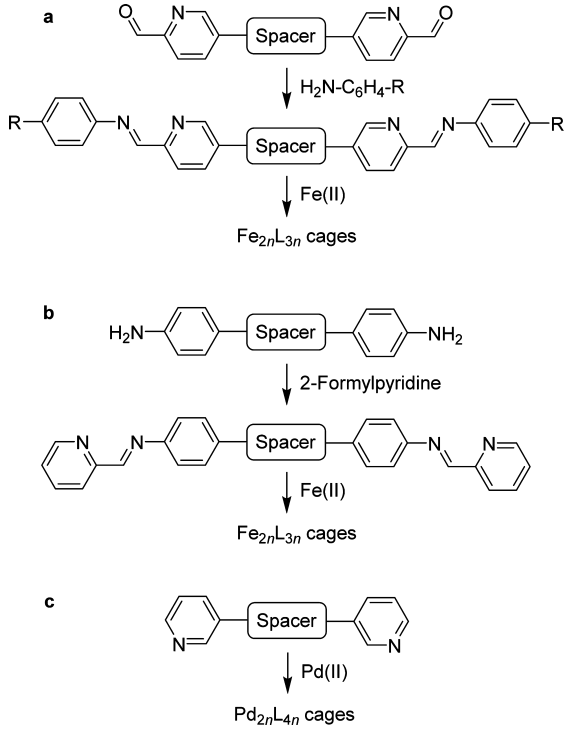

fashion, $Fe^{II}_{2n}L_{3n}$ cages are formed when ligands bearing terminal aniline groups react with 2-formylpyridine in the presence of Fe^{II} salts (Scheme 3b).[12,14] The assembly of $Pd^{II}_{2n}L_{4n}$ cages can also be achieved by the combination of linear ligands with terminal 3-pyridyl groups (Scheme 3c).[10,15,16]

In order to synthesize a clathrochelate ligand with apical formylpyridine groups, we used an acetal-protected boronic acid, the synthesis of which has been reported previously.[17] Reactions with dimethylglyoxime, nioxime, or diethylglyoxime and $FeCl_2$ in methanol produced protected clathrochelates. The yields for these reactions are modest (21, 33, and 29%, respectively) because side products are formed by a protodeboronation reaction. Clean deprotection of the acetal was achieved by a reaction with *p*-toluenesulfonic acid using microwave heating to give the target clathrochelates **1**, **2**, and **3** (Scheme 4).

For the syntheses of 4-aminophenyl-terminated clathrochelates, we also employed a protecting group strategy. Starting from (4-(dibenzylamino)phenyl)boronic acid,[18] we first synthesized the Fe^{II} clathrochelate complexes, which were

DOI: 10.1021/jacs.5b13190
J. Am. Chem. Soc. 2016, 138, 2046−2054

Scheme 4. Synthesis of the Clathrochelates 1, 2, and 3[a]

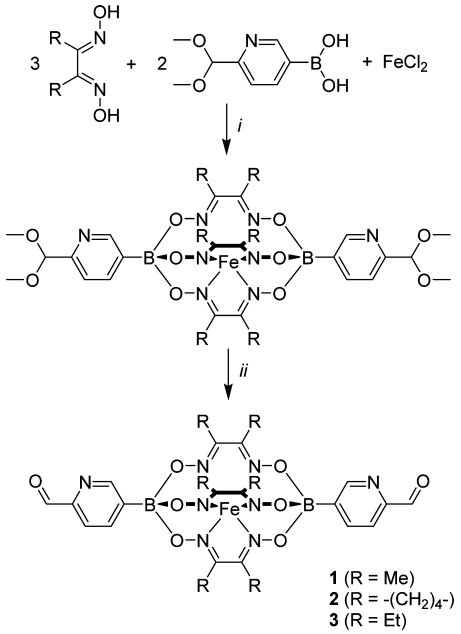

[a]Reagents and conditions: (*i*) MeOH, reflux, 4 h; (*ii*) TsOH (0.1 equiv), $CHCl_3$/*t*-BuOH (4:1), 140 °C, 4 h.

subsequently deprotected through hydrogenation to give complexes **4** and **5** with overall yields of 53% and 73%, respectively (Scheme 5).

The new clathrochelates **1**−**5** were characterized in solution by NMR spectroscopy (Figures S11−S20) and high-resolution mass spectrometry. In addition, we have analyzed the molecular structure of **1** and of the HCl adducts of **4** and **5** in the solid state by single-crystal X-ray crystallography. The structures are shown in Figure 1. The view along the B···B axis reveals the

Scheme 5. Synthesis of the Clathrochelates 4 and 5[a]

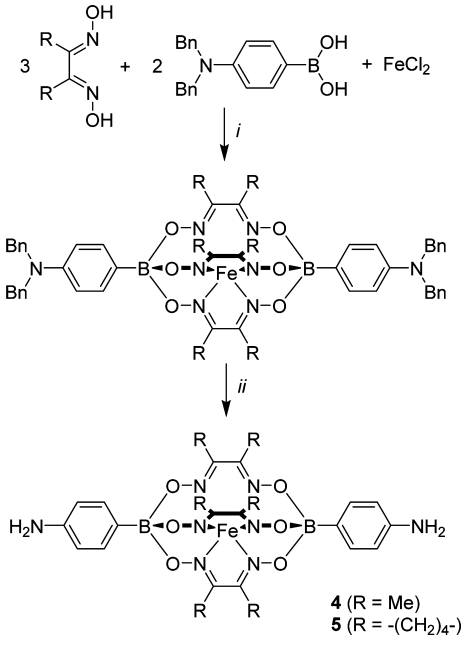

[a]Reagents and conditions: (*i*) MeOH, reflux, 4 h; (*ii*) H_2, Pd/C, MeOH/$CHCl_3$ (1.5:1), 50 °C, 4 h.

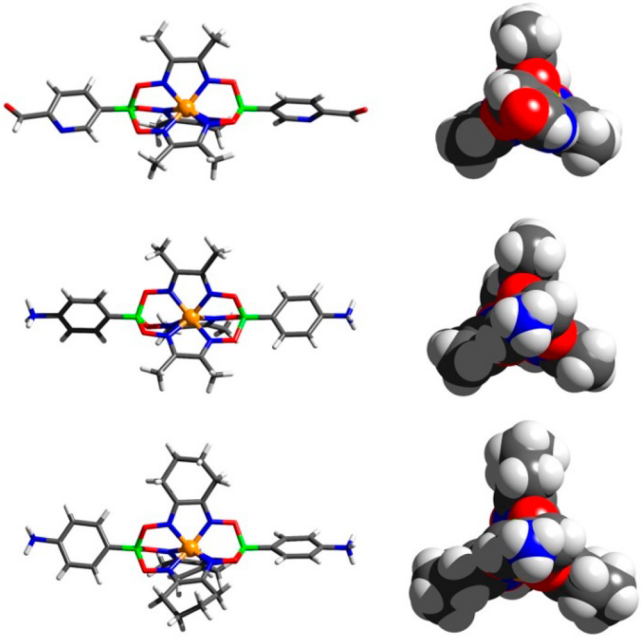

Figure 1. Molecular structures of the clathrochelates **1** (top), **4**·HCl (middle), and **5**·HCl (bottom) in the crystal. A stick representation (side view, left) and a space-filling representation (view along the B···B axis, right) are given for each complex. Chloride anions are omitted for clarity. Gray: C; white: H; dark blue: N; green: B; red: O; and orange: Fe.

pseudo C_3 symmetry of the complexes. Furthermore, it is evident that the lateral size of the nioxime-based complex **5** is significantly larger than that of the dimethylglyoxime-based complexes **1** and **4**.

The 3-pyridyl-capped clathrochelates **6**−**8** can be obtained by reaction of commercial 3-pyridylboronic acid with $FeCl_2$ and the respective dioxime ligand (Scheme 6). We have recently

Scheme 6. Synthesis of the Clathrochelates 6−8[a]

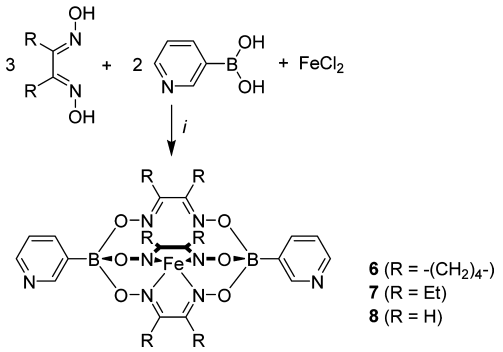

[a]Conditions: (*i*) MeOH, reflux, 4 h (**6** and **7**); TFA, reflux, 6 h (**8**).

shown that $Pd^{II}_6L_{12}$ octahedral coordination cages are formed upon combination of metalloligand **6** with Pd^{II}.[10] In order to probe if the assembly process can be influenced by the aspect ratio of clathrochelate-based ligands, we have synthesized the new ligands **7** and **8**. Clathrochelate **7** is slightly larger than the nioxime-based **6** because the six ethyl groups of **7** require more space than the three conformationally fixed -$(CH_2)_4$- rings of **6**. Clathrochelate **8**, in contrast, is the thinnest (largest aspect ratio) of the three metalloligands **6**−**8**. The difference in

DOI: 10.1021/jacs.5b13190
J. Am. Chem. Soc. 2016, 138, 2046−2054

equatorial steric bulk of **7** and **8** is evident when comparing the structures in the solid state (Figure 2).

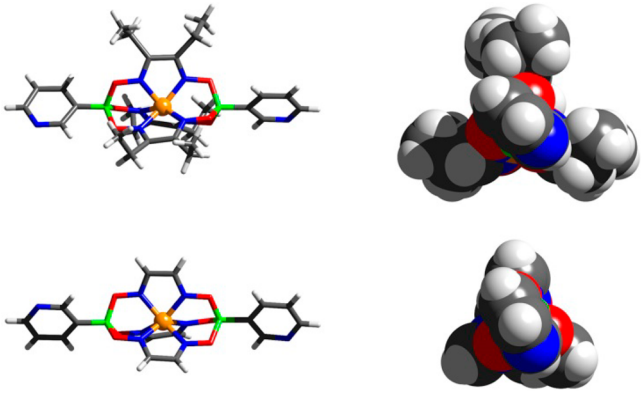

Figure 2. Molecular structures of the clathrochelates **7** (top) and **8** (bottom) in the crystal. A stick representation (side view, left) and a space-filling representation (view along the B···B axis, right) are given for each complex. Gray: C; white: H; dark blue: N; green: B; red: O; and orange: Fe.

Fe^{II}-Based Coordination Cages. The coordination cages **9**–**11** were formed by heating an acetonitrile solution containing clathrochelate **1**, **2**, or **3** (3 equiv); *p*-toluidine (6 equiv); and Fe(OTf)$_2$ or Fe(NTf$_2$)$_2$ (2 equiv) at 50 °C for 18 h (Scheme 7). Workup allowed isolation of the cages in high yield (>90%). The ^{1}H NMR spectra of the products were very complex, in particular those of cages **10** and **11** (Figures S23, S25, S27, and S29), which showed broad and ill-resolved peaks. Such behavior is not unexpected because this type of cage is often observed as a mixture of diastereoisomers with different relative stereochemistries of the iron centers at the corners.[12,19] Furthermore, the cages may not provide sufficient space for free rotation of the clathrochelate core. Restricted ligand rotation on the NMR time scale would lead to further reduction of the apparent symmetry. The DOSY NMR spectra of **9** (Figure S22), **10** (Figures S24 and S26), and **11** (Figures S28 and S30) revealed the presence of large assemblies with a uniform diffusion constant. However, the diffusion constant of **9** (4.43×10^{-6} cm^2/s) was larger than those of **10** (**10a**: 2.89×10^{-6} cm^2/s; **10b**: 2.85×10^{-6} cm^2/s) and **11** (**11a**: 2.36×10^{-6} cm^2/s; **11b**: 2.62×10^{-6} cm^2/s), even though ligands of the same lengths were employed (**1**–**3**). This result provides evidence that complexes **10** and **11** are not typical tetrahedral coordination cages, but larger assemblies.

High-resolution ESI mass spectrometry revealed that cage **9** has the composition $[Fe_4(\mathbf{L1})_6]^{8+}$ (Figure 3). The tetrahedral geometry is in line with what has been observed for other assemblies based on linear, rigid rod-type ligands with terminal formylpyridine groups.[12,13] The cages **10** and **11**, on the other hand, have the composition $[Fe_8(\mathbf{L2/3})_{12}]^{16+}$ (Figure 3 for **11b**, and S56–S66 for both).

We infer **10** and **11** to possess an approximately cubic structure, with eight iron(II) centers at its vertices. Cubic coordination cages with Fe^{II}(N,N′-chelate)$_3$ complexes as vertices have already been described.[20,21] These complexes are often based on four-fold-symmetric, face-capping ligands, and have an Fe$^{II}_8$L$_6$ stoichiometry. A cubic Fe$^{II}_8$L$_{12}$ cage has also been reported, but the coordinate vectors of its ligands are oriented at 120° with respect to each other,[21] in contrast with the parallel coordinate vectors of **L2** and **L3**. M$_8$L$_{12}$ cages with

Scheme 7. Synthesis of Coordination Cages 9–11[a]

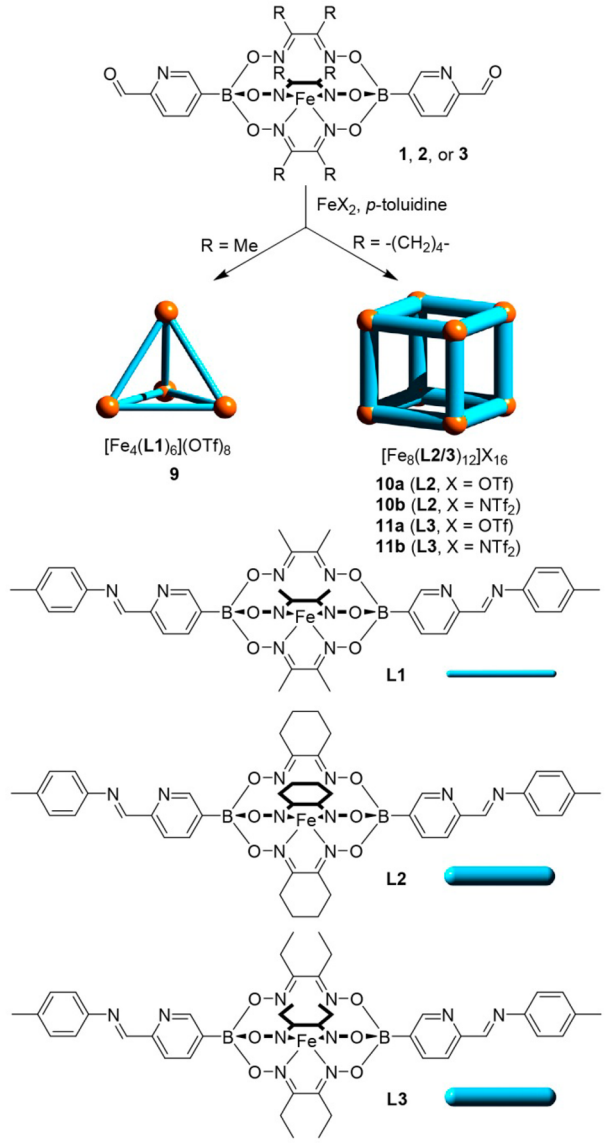

[a]Conditions: **1**, **2**, or **3** (3 equiv), Fe(OTf)$_2$ or Fe(NTf$_2$)$_2$ (2 equiv), *p*-toluidine (6 equiv), CH$_3$CN, 50 °C, 18 h.

other metal ions in the vertices (M = Cu^{II}, Zn^{II}, Ni^{II}, or Co^{II}) have also been studied.[22,23] These cages were obtained using template effects[23a] or ligands with some conformational freedom, resulting in variable coordinate vectors. In our case, the coordinate vectors of **L2** and **L3** should favor the formation of a tetrahedral Fe$^{II}_4$L$_6$ cage. The fact that we observe an entropically disfavored Fe$^{II}_8$L$_{12}$ cage instead of a tetrahedron can be attributed to the small aspect ratio of ligands **L2** and **L3**. Their lateral size is significantly larger than that of **L1**, and a tetrahedral geometry would lead to unfavorable steric interactions between the lateral -(CH$_2$)$_4$- or Et groups.

Next, we investigated the formation of coordination cages starting from the aniline-terminated clathrochelates **4** and **5**. The lateral size of these complexes is the same as for **1** and **2** (Me and -(CH$_2$)$_4$- side chains), but condensation with 2-formylpyridine results in ligands with an increased distance between the two N,N′-chelating sites (cf. Scheme 3a and 3b). The aspect ratio of the metalloligands is thus increased.

DOI: 10.1021/jacs.5b13190
J. Am. Chem. Soc. 2016, 138, 2046–2054

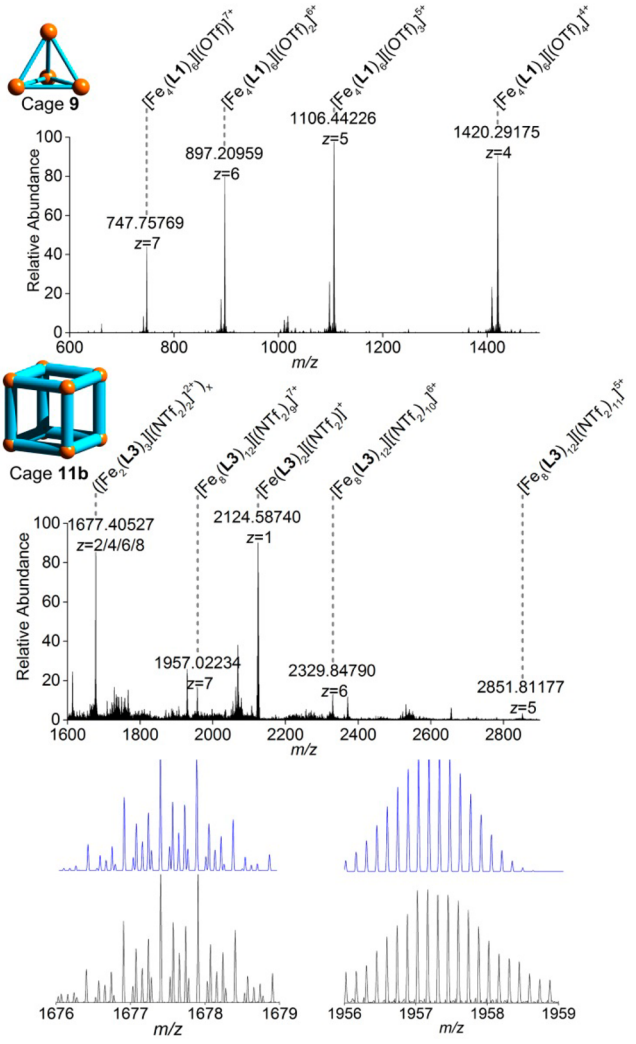

Figure 3. High-resolution ESI MS spectra of the tetrahedral cage **9** (top) and of the cubic cage **11b** (middle), along with zoom-ins on the peaks at 1677 and 1957 *m*/*z* (bottom). The simulated spectra are placed above the experimental data.

When **4** or **5** was combined with 2-formylpyridine and $Fe(OTf)_2$ or $Fe(NTf_2)_2$, DOSY spectroscopy (Figures S32, S34, and S36) indicated all products diffused at indistinguishable rates. The ^{1}H NMR spectra of cages **12** and **13** showed several sets of signals, suggesting the presence of diastereoisomers (Figures S31, S33, and S35).[12,19] Clear evidence for the stoichiometry of the cages was again obtained by high-resolution mass spectrometry (Figures S67–S69): both cages have the composition $Fe^{II}_4L_6$ (Scheme 8).

The decanuclear cages **12b** and **13** were analyzed by single-crystal X-ray diffraction (Figure 4). Both cages crystallize as a racemic mixture of ΔΔΔΛ and ΛΛΛΔ isomers, with cage **12b** showing a pseudo C_3 symmetry axis while cage **13** displays full crystallographic C_3 symmetry. The four Fe^{II}(N,N′-chelate)$_3$ complexes in the vertices have an average distance of about 20 Å. The cavity size of cage **12b** is approximately 480 Å^3 as determined by VOIDOO calculations. For cage **13**, the cavity is considerably smaller (377 Å^3) because the lateral -$(CH_2)_4$- groups block part of the space inside the cavity (Figure S83).

The formation of $Fe^{II}_4L_6$ cages with both aniline-terminated clathrochelates is consistent with the inference that aspect ratio, and not the absolute width of the ligand, is the decisive factor in

Scheme 8. Synthesis of the Coordination Cages 12 and 13[a]

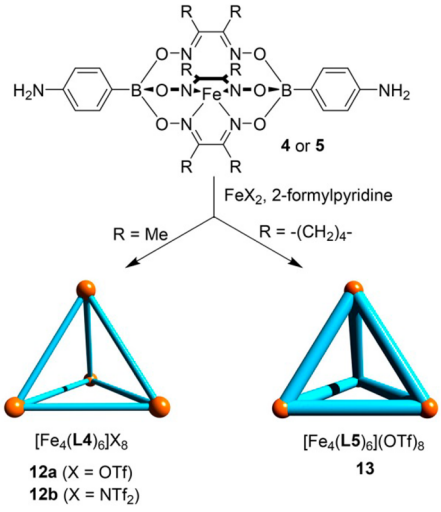

[a]Conditions: **4** or **5** (3 equiv), $Fe(OTf)_2$ or $Fe(NTf_2)_2$ (2 equiv), *p*-toluidine (6 equiv), CH_3CN, 50 °C, 18 h.

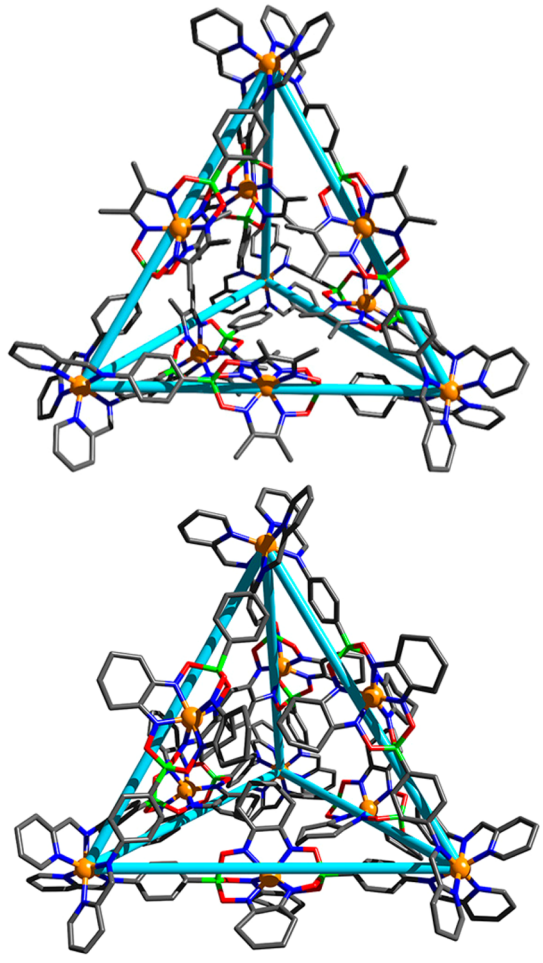

Figure 4. Molecular structures of the cages **12b** and **13** in the crystal. Hydrogen atoms, counteranions, and solvent molecules are omitted for clarity. Gray: C; dark blue: N; green: B; red: O; and orange: Fe.

controlling the geometry. In fact, ligand **L5** (the condensation product of **5** and 2-formylpyridine) and ligand **L2** have the same lateral size, but **L5** has an increased aspect ratio because

DOI: 10.1021/jacs.5b13190
J. Am. Chem. Soc. 2016, 138, 2046–2054

the metal binding sites are farther apart. As a result of this difference, we observe an $Fe^{II}_8L_{12}$ cage with **L2** but an $Fe^{II}_4L_6$ cage with **L5**.

Pd^{II}-Based Coordination Cages. The results obtained with Fe^{II}-based coordination cages prompted us to investigate whether the aspect ratio of a ligand can also influence the assembly of other types of cages. To address this question, we have focused on cages that can be obtained from Pd^{II} salts and dipyridyl ligands. As mentioned above, we have previously shown that the combination of 3-pyridyl-capped clathrochelate **6** with Pd^{II} gives an octahedral $[Pd_6(\mathbf{6})_{12}]^{12+}$ cage.[10] Metalloligand **6** has nearly the same aspect ratio as ligand **7**. We were thus not surprised that an octahedral cage (**14**) was also formed when **7** was mixed with $[Pd(CH_3CN)_4](BF_4)_2$ in acetonitrile (Scheme 9).

Scheme 9. Synthesis of the Coordination Cages 14, 15, and 17[a]

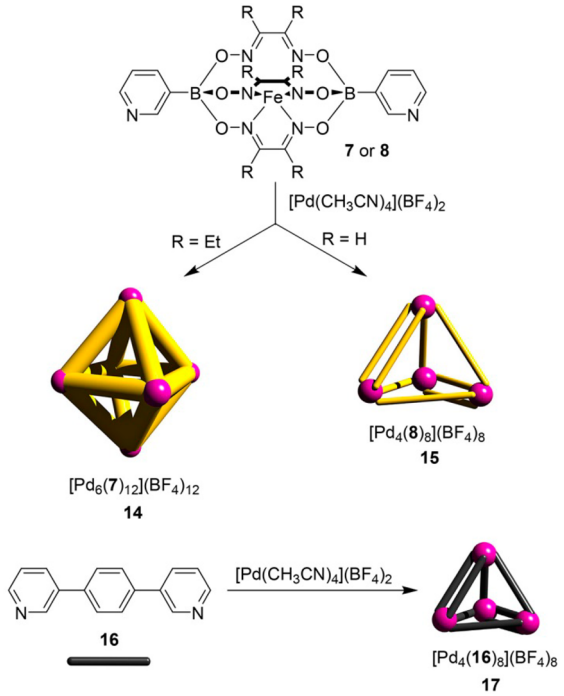

[a]Conditions: CH_3CN, 70 °C, 3 h (**12**); DMF, 70 °C, 4 d (**13**); DMSO, 90 °C, 10 min (**15**).

Cage **14** was characterized by NMR spectroscopy (Figures S47–S50), high-resolution mass spectrometry (Figure S70), and single-crystal X-ray crystallography (Figure 5). The average Pd···Pd distance within a triangular face was found to be 16.0 Å, a value which is very similar to what was observed for $[Pd_6(\mathbf{6})_{12}]^{12+}$.[10] These first results suggest that the metalloligands **6** and **7** behave very similarly in self-assembly reactions. However, we show in the next section that the small difference in the aspect ratios of **6** and **7** can have a rather pronounced effect on the dynamic behavior of Pd^{II} cages.

The reaction of metalloligand **8** with $[Pd(CH_3CN)_4](BF_4)_2$ resulted in the clean formation of coordination cage **15**. Analysis by ^{1}H NMR spectroscopy revealed a reduced symmetry: instead of one set of signals for the bridging clathrochelate ligands as found for **14**, we observed two sets of signals for **15** (Figure S51). Since the two sets of signals have equal intensity, we infer that the apparent symmetry reduction

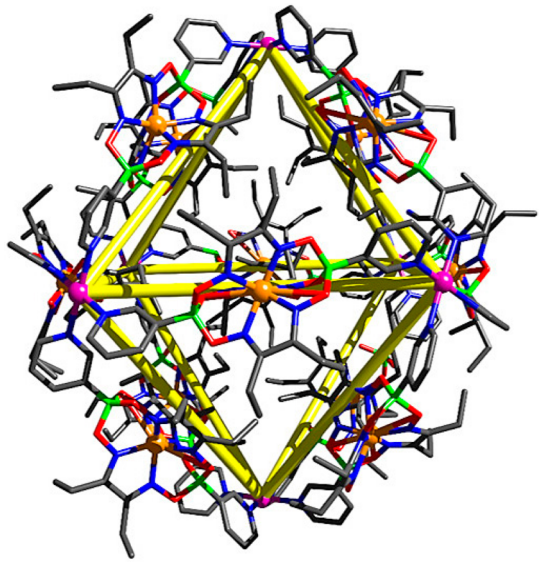

Figure 5. Molecular structure of cage **14** in the crystal. Hydrogen atoms, counteranions, and solvent molecules are omitted for clarity. Gray: C; dark blue: N; green: B; red: O; pink: Pd; and orange: Fe.

is not due to restricted rotational freedom of the bridging clathrochelate ligands. Instead, the data indicate the presence of two kinds of ligands, which are magnetically distinct. The DOSY NMR spectrum of **15** in deuterated DMSO (Figure S52) confirmed the presence of only one type of assembly with a diffusion constant of 7.64×10^{-7} cm^2/s. This value is larger than what was observed for **14** (6.14×10^{-7} cm^2/s; DMSO-d_6) (Figure S50), suggesting that **15** is a smaller assembly. This point was confirmed by high-resolution mass spectrometry, which showed that cage **15** has the formula $[Pd_4(\mathbf{8})_8]^{8+}$. The presence of a tetrahedral cage is in line with the apparent reduction of symmetry, because a tetrahedral cage should feature two doubly bridged $Pd(\mathbf{8})_2Pd$ links in addition to four singly bridged Pd(**8**)Pd connections. This geometry was indeed observed when cage **15** was analyzed by single-crystal X-ray diffraction (Figure 6). The four Pd atoms form a slightly distorted tetrahedron, with the Pd···Pd distances for the doubly

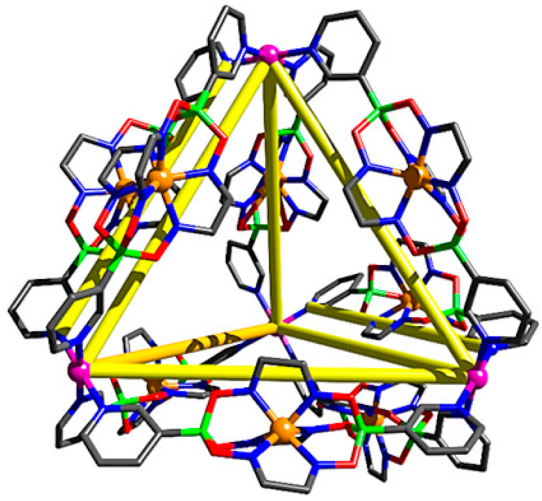

Figure 6. Molecular structure of cage **15** in the crystal. Hydrogen atoms, counteranions, and solvent molecules are omitted for clarity. Gray: C; dark blue: N; green: B; red: O; pink: Pd; and orange: Fe.

DOI: 10.1021/jacs.5b13190
J. Am. Chem. Soc. 2016, 138, 2046–2054

bridged Pd(**8**)$_2$Pd units being slightly smaller than the distances for the singly bridged Pd(**8**)Pd connections (14.7 vs 15.5 Å). The distance between the two encapsulated Fe^{II} ions in the doubly bridged Pd(**8**)$_2$Pd is only 5.7 Å, resulting in a tight packing of the two clathrochelate frameworks. For the more bulky ligand **7**, the formation of doubly bridged Pd(**7**)$_2$Pd links is expected to be unfavorable, thereby pushing the system toward an octahedral geometry which shows exclusively singly bridged Pd(**7**)Pd connections.

Overall, the structure of cage **15** resembles that of cage **17**, which is obtained by combination of "naked" Pd^{II} and the simple phenylene-bridged ligand **16** (Scheme 9). This type of cage had previously been described by the group of Fujita, albeit with different counteranions.[15] As in the case of **15**, a tetrahedral geometry is observed, with two doubly bridged edges, resulting in a double set of ^{1}H NMR signals for the ligand protons (Figure S53).

The different structures that we have observed for octahedral cage **14** on the one hand, and for the tetrahedral cages **15** and **17** on the other hand, provide further evidence that it is possible to control the geometry of coordination cages via the aspect ratio of the ligand. The difference between **14** and **15** is particularly remarkable because the cages are both based on clathrochelate ligands having exactly the same length, but just a different width.

Self-Sorting of Pd-Based Coordination Cages. The observations described in the last section suggest that there exists a fine thermodynamic balance between potential products within a simple supramolecular system consisting of Pd^{II} ions and bis(3-pyridyl) ligands, which can be decisively tipped in one direction or another by modulating a single property of the donor building block: equatorial steric bulk. In order to better understand the thermodynamic factors at play, scrambling experiments were performed, in which presynthesized samples of $[Pd_6(\mathbf{6})_{12}](BF_4)_{12}$ or $[Pd_6(\mathbf{7})_{12}](BF_4)_{12}$ (**14**) and $[Pd_4(\mathbf{16})_8](BF_4)_8$ (**17**) were combined and heated to 70 °C for 4 days. Given that the self-assembly behaviors of **6** and **7** are essentially identical (both form $Pd^{II}{}_6L_{12}$ octahedra), we were struck by the dramatic differences in the outcomes of these two simple experiments. The ^{1}H NMR spectrum of a mixture of $[Pd_6(\mathbf{6})_{12}](BF_4)_{12}$ and $[Pd_4(\mathbf{16})_8](BF_4)_8$ did not significantly change during heating, confirming that no heteroleptic products were formed by ligand scrambling (Figure S72). Conversely, the ^{1}H NMR spectrum of a mixture of $[Pd_6(\mathbf{7})_{12}](BF_4)_{12}$ and $[Pd_4(\mathbf{16})_8](BF_4)_8$ became complex, suggesting that a library of structures had formed (Figure S73).

To corroborate these results, we performed mixed-ligand self-sorting experiments. Equimolar amounts of ligands **6** and **16**, or **7** and **16**, along with a corresponding amount of $[Pd(MeCN)_4](BF_4)_2$, were combined in CD_3CN and allowed to reach thermodynamic equilibrium by heating for 8 days at 50 °C. The results obtained from these experiments were in agreement with those of the scrambling experiments described above. In the presence of Pd^{II} ions, the ^{1}H NMR spectrum of a mixture of ligands **6** and **16** exclusively showed two distinct sets of peaks that clearly corresponded to the assemblies $[Pd_6(\mathbf{6})_{12}]^{12+}$ and $[Pd_4(\mathbf{16})_8]^{8+}$ (Figure 7). Such behavior can be described as "narcissistic self-sorting".[24]

In contrast, the ^{1}H NMR spectrum of a mixture of ligands **7** and **16** in the presence of Pd^{II} ions showed multiple sets of peaks, indicating that a library of products had formed (Figure 8). The presence of heteroleptic assemblies was confirmed by ESI MS analysis, wherein peaks corresponding to

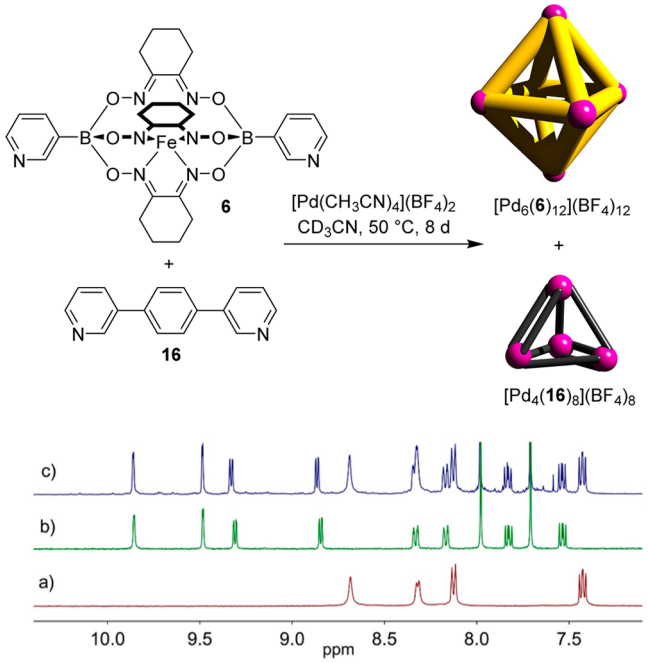

Figure 7. ^{1}H NMR spectra in CD_3CN of (a) $[Pd_6(\mathbf{6})_{12}](BF_4)_{12}$, (b) $[Pd_4(\mathbf{16})_8](BF_4)_8$, and (c) a mixture of $[Pd(MeCN)_4](BF_4)_2$ and both ligands **6** and **16** after heating for 8 days at 50 °C.

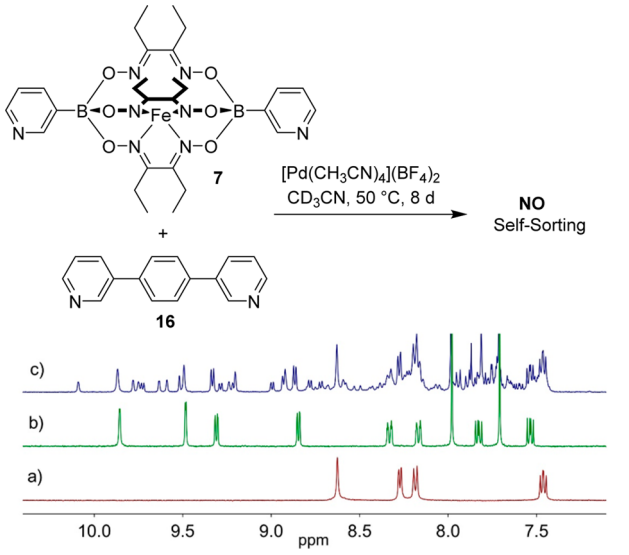

Figure 8. ^{1}H NMR spectra in CD_3CN of (a) $[Pd_6(\mathbf{7})_{12}](BF_4)_{12}$, (b) $[Pd_4(\mathbf{16})_8](BF_4)_8$, and (c) a mixture of $[Pd(MeCN)_4](BF_4)_2$ and both ligands **7** and **16** after heating for 8 days at 50 °C.

$[Pd_6(\mathbf{7})_{11}(\mathbf{16})]^{12+}$, $[Pd_6(\mathbf{7})_{10}(\mathbf{16})_2]^{12+}$, $[Pd_6(\mathbf{7})_9(\mathbf{16})_3]^{12+}$, $[Pd_6(\mathbf{7})_8(\mathbf{16})_4]^{12+}$, and $[Pd_4(\mathbf{7})_5(\mathbf{16})_7]^{8+}$ were all observed (Figures S79 and S80).

The observation that comprehensive narcissistic self-sorting occurs following mixture of ligand **6**, ligand **16**, and Pd^{II}, whereas a multicomponent library of products is observed in the case of ligand **7**, ligand **16**, and Pd^{II}, is remarkable for two reasons. First, the difference between the aspect ratios of metalloligands **6** and **7** is small, essentially arising due to the greater rotational freedom of the ethyl side chains of **7** when compared to the -$(CH_2)_4$- groups of **6**. The molecular masses of **6** (654.09 g mol^{-1}) and **7** (660.13 g mol^{-1}) differ by only

DOI: 10.1021/jacs.5b13190
J. Am. Chem. Soc. 2016, 138, 2046−2054

1%. Second, the structural differences between the ligands **6** and **7** are found far from the pyridine donor groups.

We hypothesize that the origin of the different self-sorting behavior lay in the relative thermodynamic stability of the assemblies $[Pd_6(\mathbf{6})_{12}]^{12+}$ and $[Pd_6(\mathbf{7})_{12}]^{12+}$. If the former were less stable than the latter, this would facilitate the formation of a library of products in the presence of $[Pd_4(\mathbf{16})_8]^{8+}$. Disassembly experiments were undertaken as follows in order to test this hypothesis. A solution of $[Pd_6(\mathbf{6})_{12}]^{12+}$ or $[Pd_6(\mathbf{7})_{12}]^{12+}$ in CD_3CN was treated with 24 equiv of pyridine-d_5 (Scheme 10).

Scheme 10. Differences in Thermodynamic Stability Are Revealed in Destruction Experiments with Pyridine-d_5

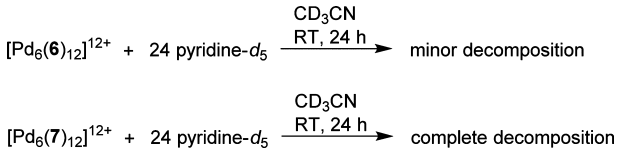

After equilibration for 24 h, the ^{1}H NMR spectrum of the solution containing $[Pd_6(\mathbf{6})_{12}]^{12+}$ showed the signals of the assembly itself, along with small signals corresponding to free ligand **6** (Figure S81). Integration of the signals revealed that only 20% of the cage had disassembled. In contrast, the ^{1}H NMR spectrum of the solution initially containing $[Pd_6(\mathbf{7})_{12}]^{12+}$ indicated the near-complete destruction of the cage. The main signals in the spectrum are attributed to the free ligand **7**, and several minor signals are likely due to Pd complexes containing both pyridine-d_5 and ligand **7** (Figure S82). These results confirm that there is indeed a pronounced difference in thermodynamic stability between the cages $[Pd_6(\mathbf{6})_{12}]^{12+}$ and $[Pd_6(\mathbf{7})_{12}]^{12+}$, even though the ligands **6** and **7** are structurally very similar. During self-sorting experiments, the steric strain of $[Pd_6(\mathbf{7})_{12}]^{12+}$ is mitigated by the incorporation of ligand **16** into heteroleptic octahedral complexes, as evidenced by the ESI MS data (Figures S78 and S80).

CONCLUSION

The size and the geometry of a ligand are of pivotal importance for metal-based self-assembly reactions. However, the ligand aspect ratio is a parameter which is rarely discussed in this context. We have shown that the aspect ratio can be used as an element of control during the formation of coordination cages. For two different types of cages, we have observed a switch toward a higher nuclearity structure when the length-to-width ratio of the ligand was reduced. In the case of Fe^{II}-based cages, we have obtained an unusual $Fe^{II}{}_8L_{12}$ structure instead of the common $Fe^{II}{}_4L_6$ tetrahedron when a ligand with a small aspect ratio was employed. In the case of Pd^{II}-based cages, we have found that we can form $Pd^{II}{}_4L_8$ or $Pd^{II}{}_6L_{12}$ cages, depending on the aspect ratio of the ligand. Intramolecular steric interactions between the ligands are likely responsible for these changes in geometry. The reduced intraligand interactions in the larger cages are enthalpically favorable, thereby compensating for the entropic penalty associated with the formation of assemblies of higher nuclearity.

Even minor differences in ligand aspect ratio can have a distinct effect on the thermodynamic stability of a coordination cage. This fact was demonstrated by disassembly experiments with two $Pd^{II}{}_6L_{12}$ cages. The ligands of these cages have the same coordinate vector orientation and length, and differ only very slightly in their equatorial steric bulk (-$(CH_2)_4$- vs 2 × -C_2H_5). The pyridine-induced disassembly was more pronounced for the cage featuring a slightly thicker ligand (smaller aspect ratio). This difference in stability was found to manifest itself in the self-sorting behavior of dynamic mixtures of $Pd^{II}{}_4L_8$ and $Pd^{II}{}_6L_{12}$ cages. Using the less stable $Pd^{II}{}_6L_{12}$ cage gave rise to a complex mixture of products, whereas narcissistic self-sorting was observed for the more stable $Pd^{II}{}_6L_{12}$ cage.

Overall, our results provide clear evidence that the aspect ratio of a rigid rod-type ligand can be an important parameter for metal-based self-assembly reactions. In order to use this parameter as an element of control, it is desirable to employ a ligand which allows modulation of its aspect ratio without too much synthetic effort. Clathrochelate-based metalloligands appear ideally suited for this purpose because their lengths, widths, and functionalities can be varied easily. Further studies with this versatile class of ligands will be reported in due course.

ASSOCIATED CONTENT

Supporting Information

The Supporting Information is available free of charge on the ACS Publications website at DOI: 10.1021/jacs.5b13190.

Experimental procedures, analytical data of the ligands and the cages (^{1}H, ^{13}C, DOSY, HRMS), and further experimental details (PDF)
X-ray crystallography data for **1** (CIF; CCDC 1442394)
X-ray crystallography data for **4** (CIF; CCDC 1442248)
X-ray crystallography data for **5** (CIF; CCDC 1442090)
X-ray crystallography data for **7** (CIF; CCDC 1442226)
X-ray crystallography data for **8** (CIF; CCDC 1442089)
X-ray crystallography data for **12b** (CIF; CCDC 1442396)
X-ray crystallography data for **13** (CIF; CCDC 1442397)
X-ray crystallography data for **14** (CIF; CCDC1415027)
X-ray crystallography data for **15** (CIF; CCDC 1442395)

AUTHOR INFORMATION

Corresponding Authors

*jrn34@cam.ac.uk
*kay.severin@epfl.ch

Author Contributions

¶S.J. and G.C. contributed equally.

Notes

The authors declare no competing financial interest.

ACKNOWLEDGMENTS

The work was supported by the Swiss National Science Foundation, by the Ecole Polytechnique Fédérale de Lausanne (EPFL), and by the Marie Curie Initial Training Networks "ReAd" and "Dynamol". We are grateful to the Swiss-Norwegian Beamline Consortium for providing access to synchrotron radiation.

REFERENCES

(1) (a) Cook, T. R.; Stang, P. J. *Chem. Rev.* **2015**, *115*, 7001−7045. (b) Lifschitz, A. M.; Rosen, M. S.; McGuirk, C. M.; Mirkin, C. A. *J. Am. Chem. Soc.* **2015**, *137*, 7252−7261. (c) Han, Y.-F.; Jin, G.-X. *Acc. Chem. Res.* **2014**, *47*, 3571−3579. (d) Young, N. J.; Hay, B. P. *Chem. Commun.* **2013**, *49*, 1354−1379. (e) Amouri, H.; Desmarets, C.; Moussa, J. *Chem. Rev.* **2012**, *112*, 2015−2041. (f) Chakrabarty, R.; Mukherjee, P. S.; Stang, P. J. *Chem. Rev.* **2011**, *111*, 6810−6918.

DOI: 10.1021/jacs.5b13190
J. Am. Chem. Soc. 2016, 138, 2046−2054

(g) Wiester, M. J.; Ulmann, P. A.; Mirkin, C. A. *Angew. Chem., Int. Ed.* **2011**, *50*, 114−137. (h) Jin, P.; Dalgarno, S. J.; Atwood, J. L. *Coord. Chem. Rev.* **2010**, *254*, 1760−1768. (i) Therrien, B. *Eur. J. Inorg. Chem.* **2009**, 2445−2453. (j) Saalfrank, R. W.; Maid, H.; Scheurer, A. *Angew. Chem., Int. Ed.* **2008**, *47*, 8794−8824. (k) Tranchemontagne, D. J.; Ni, Z.; O'Keeffe, M.; Yaghi, O. M. *Angew. Chem., Int. Ed.* **2008**, *47*, 5136−5147. (l) Dalgarno, S. J.; Power, N. P.; Atwood, J. L. *Coord. Chem. Rev.* **2008**, *252*, 825−841.

(2) Harris, K.; Fujita, D.; Fujita, M. *Chem. Commun.* **2013**, *49*, 6703−6712.

(3) Mukherjee, S.; Mukherjee, P. S. *Chem. Commun.* **2014**, *50*, 2239−2248.

(4) (a) Saha, M. L.; Neogi, S.; Schmittel, M. *Dalton Trans.* **2014**, *43*, 3815−3843. (b) Zhao, L.; Northrop, B. H.; Zheng, Y.-R.; Yang, H.-B.; Lee, H. J.; Lee, Y. M.; Park, J. Y.; Chi, K.-W.; Stang, P. J. *J. Org. Chem.* **2008**, *73*, 6580−6586. (c) Yoshizawa, M.; Nakagawa, J.; Kumazawa, K.; Nagao, M.; Kawano, M.; Ozeki, T.; Fujita, M. *Angew. Chem., Int. Ed.* **2005**, *44*, 1810−1813. (d) Yoshizawa, M.; Nagao, M.; Kumazawa, K.; Fujita, M. *J. Organomet. Chem.* **2005**, *690*, 5383−5388. (e) Grote, Z.; Scopelliti, R.; Severin, K. *Angew. Chem., Int. Ed.* **2003**, *42*, 3821−3825.

(5) Johnson, A. M.; Wiley, C. A.; Young, M. C.; Zhang, X.; Lyon, Y.; Julian, R. R.; Hooley, R. J. *Angew. Chem., Int. Ed.* **2015**, *54*, 5641−5645.

(6) Voloshin, Y. Z.; Kostromina, N. A.; Krämer, R. K. *Clathrochelates. Synthesis, Structure and Properties*; Elsevier: Amsterdam, 2002.

(7) (a) Li, L.; Fanna, D. J.; Shepherd, N. D.; Lindoy, L. F.; Li, F. *J. Inclusion Phenom. Macrocyclic Chem.* **2015**, *82*, 3−12. (b) Wise, M. D.; Severin, K. *Chimia* **2015**, *69*, 191−195.

(8) (a) Zelinskii, G. E.; Belov, A. S.; Lebed, E. G.; Vologzhanina, A. V.; Novikov, V. V.; Voloshin. *Inorg. Chim. Acta* **2016**, *440*, 154−164. (b) Lebed, E. G.; Belov, A. S.; Dolganov, A. V.; Vologzhanina, A. V.; Szebesczyk, A.; Gumienna-Kontecka, E.; Kozlowski, H.; Bubnov, Y. N.; Dubey, I. Y.; Voloshin, Y. Z. *Inorg. Chem. Commun.* **2013**, *30*, 53−57. (c) Lebed, E. G.; Belov, A. S.; Dolganov, A. V.; Vologzhanina, A. V.; Novikov, V. V.; Kuznetsov, E. V.; Voloshin, Y. Z. *Inorg. Chem. Commun.* **2013**, *33*, 57−62.

(9) (a) Zhang, Y.-Y.; Lin, Y.-J.; Jin, G.-X. *Chem. Commun.* **2014**, *50*, 2327−2329. (b) Wise, M. D.; Ruggi, A.; Pascu, M.; Scopelliti, R.; Severin, K. *Chem. Sci.* **2013**, *4*, 1658−1662.

(10) Wise, M. D.; Holstein, J. J.; Pattison, P.; Besnard, C.; Solari, E.; Scopelliti, R.; Bricogne, G.; Severin, K. *Chem. Sci.* **2015**, *6*, 1004−1010.

(11) Ardavan, A.; Bowen, A. M.; Fernandez, A.; Fielding, A. J.; Kaminski, D.; Moro, F.; Muryn, C. A.; Wise, M. D.; Ruggi, A.; McInnes, E. J. L.; Severin, K.; Timco, G. A.; Timmel, C. R.; Tuna, F.; Whitehead, G. F. S.; Winpenny, R. E. P. *npj Quantum Inf.* **2015**, *1*, 15012.

(12) (a) Zarra, S.; Wood, D. M.; Roberts, D. A.; Nitschke, J. R. *Chem. Soc. Rev.* **2015**, *44*, 419−432. (b) Smulders, M. M. J.; Riddell, I. A.; Browne, C.; Nitschke, J. R. *Chem. Soc. Rev.* **2013**, *42*, 1728−1754. (c) Ronson, T. K.; Zarra, S.; Black, S. P.; Nitschke, J. R. *Chem. Commun.* **2013**, *49*, 2476−2490.

(13) For selected examples see: (a) Roberts, D. A.; Pilgrim, B. S.; Cooper, J. D.; Ronson, T. K.; Zarra, S.; Nitschke, J. R. *J. Am. Chem. Soc.* **2015**, *137*, 10068−10071. (b) Riddell, I. A.; Ronson, T. K.; Nitschke, J. R. *Chem. Sci.* **2015**, *6*, 3533−3537. (c) Wood, C. S.; Ronson, T. K.; Belenguer, A. M.; Holstein, J. J.; Nitschke, J. R. *Nat. Chem.* **2015**, *7*, 354−358.

(14) For selected examples see: (a) Ronson, T. K.; Roberts, D. A.; Black, S. P.; Nitschke, J. R. *J. Am. Chem. Soc.* **2015**, *137*, 14502−14512. (b) Foster, J. A.; Parker, R. M.; Belenguer, A. M.; Kishi, N.; Sutton, S.; Abell, C.; Nitschke, J. R. *J. Am. Chem. Soc.* **2015**, *137*, 9722−9729. (c) Wood, D. M.; Meng, W.; Ronson, T. K.; Stefankiewicz, A. R.; Sanders, J. K. M.; Nitschke, J. R. *Angew. Chem., Int. Ed.* **2015**, *54*, 3988−3992. (d) Ronson, T. K.; League, A. B.; Gagliardi, L.; Cramer, C. J.; Nitschke, J. R. *J. Am. Chem. Soc.* **2014**, *136*, 15615−15624.

(15) Chand, D. K.; Biradha, K.; Kawano, M.; Sakamoto, S.; Yamaguchi, K.; Fujita, M. *Chem. - Asian J.* **2006**, *1*, 82−90.

(16) For cages based on bent (instead of linear) ligands see: Han, M.; Engelhard, D. M.; Clever, G. H. *Chem. Soc. Rev.* **2014**, *43*, 1848−1860.

(17) Sørensen, A.; Castilla, A. M.; Ronson, T. K.; Pittelkow, M.; Nitschke, J. *Angew. Chem., Int. Ed.* **2013**, *52*, 11273−11277.

(18) Kalinin, A.; Lehnemann, B.; Meudt, A.; Scherer, S.; Sniekus, V. European Patent EP 1479686 A1.

(19) (a) Castilla, A. M.; Ramsay, W. J.; Nitschke, J. R. *Acc. Chem. Res.* **2014**, *47*, 2063−2073. (b) Castilla, A. M.; Ramsay, W. J.; Nitschke, J. R. *Chem. Lett.* **2014**, *43*, 256−263.

(20) (a) Ramsay, W. J.; Szczypiński, F. T.; Weissman, H.; Ronson, T. K.; Smulders, M. M. J.; Rybtchinski, B.; Nitschke, J. R. *Angew. Chem., Int. Ed.* **2015**, *54*, 5636−5640. (b) Ramsay, W. J.; Ronson, T. K.; Clegg, J. K.; Nitschke, J. R. *Angew. Chem., Int. Ed.* **2013**, *52*, 13439−13443. (c) Otte, M.; Kuijpers, P. F.; Troeppner, O.; Ivanović-Burmazović, I.; Reek, J. N. H.; de Bruin, B. *Chem. - Eur. J.* **2013**, *19*, 10170−10178. (d) Meng, W.; Breiner, B.; Rissanen, K.; Thoburn, J. D.; Clegg, J. K.; Nitschke, J. R. *Angew. Chem., Int. Ed.* **2011**, *50*, 3479−3483.

(21) Browne, C.; Brenet, S.; Clegg, J. K.; Nitschke, J. R. *Angew. Chem., Int. Ed.* **2013**, *52*, 1944−1948.

(22) Ward, M. D. *Chem. Commun.* **2009**, 4487−4499.

(23) (a) Riddell, I. A.; Hristova, Y. R.; Clegg, J. K.; Wood, C. S.; Breiner, B.; Nitschke, J. R. *J. Am. Chem. Soc.* **2013**, *135*, 2723−2733. (b) Stephenson, A.; Ward, M. D. *Dalton Trans.* **2011**, *40*, 10360−10369. (c) Najar, A. M.; Tidmarsh, I. S.; Adams, H.; Ward, M. D. *Inorg. Chem.* **2009**, *48*, 11871−11881. (d) Argent, S. P.; Adams, H.; Harding, L. P.; Ward, M. D. *Dalton Trans.* **2006**, 542−544. (e) Bell, Z. R.; Harding, L. P.; Ward, M. D. *Chem. Commun.* **2003**, 2432−2433.

(24) (a) He, Z.; Jiang, W.; Schalley, C. A. *Chem. Soc. Rev.* **2015**, *44*, 779−789. (b) Isaacs, L. *Acc. Chem. Res.* **2014**, *47*, 2052−2062. (c) Lal Saha, M.; Schmittel, M. *Org. Biomol. Chem.* **2012**, *10*, 4651−4684. (d) Safont-Sempere, M. M.; Fernández, G.; Würthner, F. *Chem. Rev.* **2011**, *111*, 5784−5814.

DOI: 10.1021/jacs.5b13190
J. Am. Chem. Soc. 2016, 138, 2046−2054